DOI 10.1515/aot-2014-0003 — Adv. Opt. Techn. 2014; 3(2): 187–197

Research Article

Lars Sjöqvist*, Markus Henriksson, Per Jonsson and Ove Steinvall

Time-correlated single-photon counting range profiling and reflectance tomographic imaging

Abstract: Time-correlated single-photon counting (TCSPC) range profiling and imaging provide high resolution laser radar data applicable in several optical remote sensing applications at short and long distances. Excellent range resolution, below centimetres, can be obtained and information about remote objects can be extracted from TCSPC range profiles. The present study describes a TCSPC range profiling system with subcentimetre range resolution applied for remote sensing of objects at short and longer ranges. Experimental results from interrogation of geometrical shapes, reflectance tomographic imaging and range profiling at longer distance in daylight conditions are presented.

Keywords: imaging; range profiling; time-correlated single-photon counting; tomography; turbulence.

***Corresponding author: Lars Sjöqvist,** Laser Systems Group, Division of Sensor and EW Systems, Swedish Defence Research Agency, FOI, P.O. Box 1165, SE 581 11, Linköping, Sweden, e-mail: larsjo@foi.se
Markus Henriksson, Per Jonsson and Ove Steinvall: Laser Systems Group, Division of Sensor and EW Systems, Swedish Defence Research Agency, FOI, P.O. Box 1165, SE 581 11, Linköping, Sweden

1 Introduction and background

High-resolution laser radar (or LAser Detection And Ranging – LADAR) techniques exhibit several interesting features for ranging and three-dimensional (3D) imaging at short and longer distances [1]. Applications range from, for example, classification and recognition of remote targets, terrain mapping, range profiling, bathymetry, robotic vision and industrial optical metrology. The recent development of single-photon counting detectors based on single pixel devices and smaller focal plane arrays have provided new opportunities and have advanced the field [2, 3]. In particular, schemes utilising time-correlated single-photon counting (TCSPC) have been shown to provide excellent range resolution on the order of centimetres or better [4, 5]. In comparison to traditional burst illumination and 3D LADAR based on linear-mode avalanche photodiode detectors (APDs) TCSPC exhibits advantages such as extreme accuracy and range resolution, easy access to multiple surface return signals via the histogram and the possibility to use high-pulse repetition rate laser sources with low-pulse energy.

The TCSPC range profiling and LADAR scheme is based on the time-of-flight (TOF) approach measuring the time required for the photons to travel from the laser transmitter to the target and back to the receiver. In TCSPC this is accomplished by carefully measuring the time between a laser pulse sync signal and registration of a single-photon event of photons reflected from a target. The measurement is performed multiple times and a histogram of arrival times is computed to gain information about surfaces at different distances within the field of view and to exclude spurious detections from detector and background noise. Systems using moderate pulse repetition rates and a limited number of acquisitions are usually called Geiger-mode APD (GM-APD) laser radar [6], whereas systems using laser pulse repetition rates in the MHz range, that is, more acquisitions and lower detection probabilities, are termed TCSPC laser radar with single-photon avalanche photodiode (SPAD) detectors.

The technology development of actively quenched SPAD detectors has advanced the field of TCSPC applications [7–9]. Single pixel silicon-based SPAD devices offer shot-noise limited detection, high quantum efficiency in a broad spectral region, low timing jitter, low dark current and robustness against high light levels. Eye safety has encouraged the development of single-photon detectors in the short wave infrared wavelength (SWIR) region based on InGaAsP materials [10]. Pulsed semiconductor and mode-locked fibre lasers with pulse repetition frequencies of tenths of MHz and picosecond pulse duration provides excellent sources for TCSPC LADAR [11]. Fibre lasers are brought to suitable wavelengths for

Si-SPAD detection by frequency doubling or super continuum generation.

A multiple-wavelength TCSPC system was assembled and described by Buller and co-workers showing detection of corner cube retro reflectors at up to 17 km range in full daylight conditions [12, 13]. Theoretical methods for extracting information from non-cooperative targets based on maximum likelihood estimation and reversible jump Markov Chain Monte Carlo (RJMCMC) algorithms were developed and shown to provide good agreement with experimental results [14]. More recently, the Bayesian analysis based on RJMCMC has been applied to analyse full waveform 3D TCSPC data [15].

High-resolution TCSPC 3D imaging at near infrared (NIR) wavelengths has been comprehensively explored at longer ranges, studying both cooperative and non-cooperative distributed objects, and has been reviewed by Buller and Wallace [4]. The scanning in the lateral plane was accomplished using a pair of galvanic mirrors. A method to overcome the range ambiguity problem in TCSPC imaging was presented showing centimetre range accuracy at 50 m and 4.4 km [16]. Krichel et al. also proposed a novel method for generation of 3D data utilising a cumulative acquisition approach building up depth information from several lateral frames [17].

For more rapid imaging parallelisation by the use of detectors in a focal plane array (FPA) architecture is necessary. GM-APDs in FPA configurations for 3D LADAR mapping, target detection and foliage penetration applications have been studied in the Jigsaw programme [18], implemented on un-manned aerial platforms [19] and demonstrated in topographic and bathymetric imaging [20]. Recently, a 3D 32×32 GM-APD LADAR camera was demonstrated on different platforms, for example, terrain mapping and reconnaissance [21]. So far, 32×32 GM-APD FPAs have been investigated for airborne 3D applications but larger arrays, using 32×128 pixels, are under development [22, 23]. Recently, several new detector approaches and TCSPC TOF schemes for 3D imaging have been reported [24]. High-altitude airborne LADAR based on single-pixel and FPA SPAD detectors have been analysed by Hiskett and Lamb [25].

Other methods for rapid single-photon counting 3D laser radar include using a single-pixel detector and compressed sensing (CS) for lateral image reconstruction, which has been studied by Howland and co-workers [26, 27]. CS provides an alternative scheme for 3D depth imaging in comparison to mechanically scanning an instantaneous field-of-view (FOV). Using CS, a pixel resolution of 256×256 was demonstrated using relatively short reconstruction times and if the lateral resolution was decreased to 32×32 a video rate at 14 frames/s was achieved [27].

Superconducting nanowire single-photon detectors (SNSPDs) operating at 1560 nm have been utilised in TOF scanning imaging experiments at long range up to approximately 1 km studying non-cooperative objects. The system exhibited a timing jitter of 100 ps providing resolution of the order of centimetres in daylight experiments [28]. Using an SNSPD in a TCSPC TOF experiment at 1550 nm wavelength, even lower timing resolution, 27 ps, was recently demonstrated providing a depth resolution of 4 mm at 115 m range [29]. Laser ranging has also been reported using a 1 GHz gated InGaAs/InP APD resulting in 8 cm range resolution in daylight conditions [30].

Examples of studied auxiliary applications using a TCSPC scheme include optical quantum key distribution [31], underwater optical communication [32], gun muzzle flash detection [33] and target discrimination in optical augmentation [34].

In this study, we present experimental results using TCSPC laser radar in high-resolution range profiling and reflectance tomography in laboratory experiments and outdoor measurements at longer distances. High-resolution range profiling can be used to remotely extract information about geometric shapes, classify optical assemblies and acquire tomographic information of rotating objects. Subcentimetre resolution range profiling of retro-reflecting targets is demonstrated at ranges of up to 750 m in daylight conditions.

2 Experimental system

The TCSPC system consists of several important parts, the short pulse laser, the transceiver for emitting the laser pulses and collecting the reflected photons, the single-photon detection module and the timing acquisition hardware. Two different transceivers have been used in the TCSPC experiments: one wide FOV setup for indoor laboratory experiments at shorter range using a bistatic configuration (setup A in Figure 1) and one narrow FOV monostatic configuration (setup B in Figure 1) for outdoor long range experiments in daylight conditions.

2.1 Hardware description

The basic TCSPC hardware used in all experimental setups was identical. The laser source was a super continuum (SC)

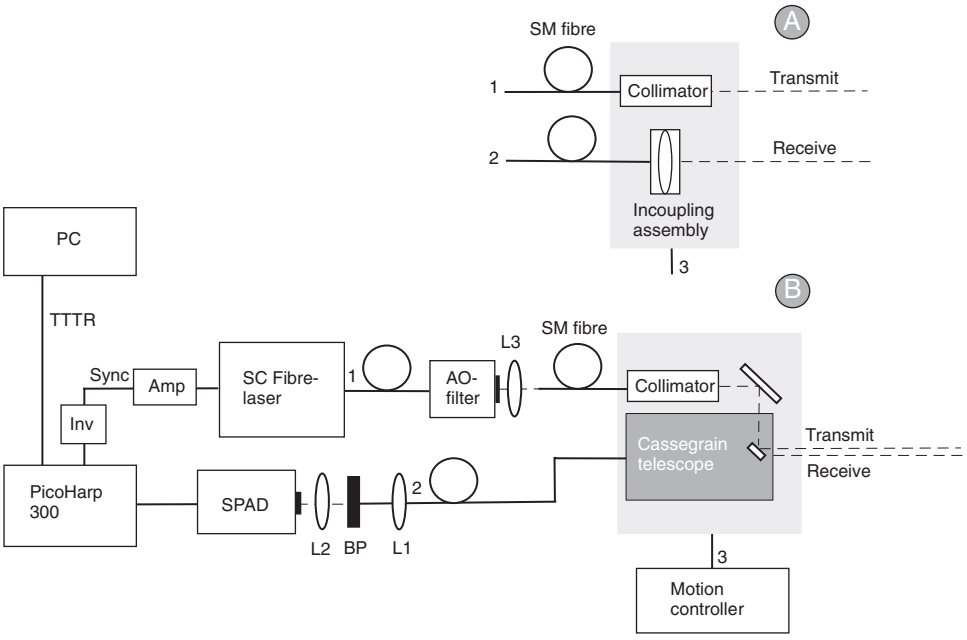

Figure 1 Experimental setup used for indoor and outdoor TCSPC experiments. Panels (A) and (B) correspond to the bistatic and monostatic setups, respectively. Both transmit/receive assemblies were mounted on turn tables (rotational and goniometer stages). Abbreviations: SM, single mode; SC, super continuum; Amp, amplifier; Inv, inverter; SPAD, single photon avalanche diode; L1, collimating lens; L2/L3, focussing lenses; Sync, laser pulse sync signal; TTTR, time-tagged time-resolved signal; AO, acousto-optical.

fibre laser (SC450, Fianium Ltd., Southampton, UK) with 4 ps pulse duration operating at 40 MHz pulse repetition frequency (PRF). In general, an SC continuum fibre laser may operate at different PRFs affecting the pulse-to-pulse interval and the ambiguity distance in TOF TCSPC applications (see below). The SC fibre laser emits radiation in a continuum, ranging from 450 to 1900 nm, although in this study only a fixed wavelength band in the NIR wavelength region was used.

2.2 Wide FOV transceiver

In the wide FOV setup, the permanently mounted collimator head of the laser output fibre was used to direct the laser beam towards the target. The receiver channel consisted of a short focal length lens focusing the reflected photons into a 62.5 μm core graded index (GRIN) multimode fibre for coupling to the detector module. The transceiver used a bistatic configuration (Figure 1) with the optical axes of transmit and receive channels separated by 70 mm vertically. The system FOV was 6.2 mrad FWHM (full width at half maximum). This bistatic configuration was used in indoor studies of geometrical shapes and for performing reflectance TCSPC tomography.

2.3 Narrow FOV transceiver

To allow outdoor experiments without laser safety restrictions, an acousto-optical (AO) filter operating between 650 and 1100 nm was used to select the wavelength of the laser and reduce the total transmitted power. The output from the AO filter was focussed into a single-mode fibre for transmission to the transceiver and subsequently collimated by a single lens. The receiver channel consisted of a Cassegrain telescope with 500 mm focal length and 125 mm aperture diameter, which focussed the collected photons into the GRIN fibre. The transmit channel was physically isolated from the receiver by a 45° outcoupling mirror, which was attached to the telescope central obscuration providing a monostatic configuration, according to Figure 1. The fibre positions could be adjusted to change the focussing distance from short ranges of below 50 m, useful for acquisition of high-resolution 3D scenes by mechanical scanning of the whole transceiver head, to long ranges of several kilometres for interrogation of retroreflecting targets. The FOV of the monostatic system was 120 μrad (FWHM) and the beam divergence was adjusted to coincide with the receiver FOV.

Both optical setups (wide and narrow FOVs) were mounted on rotational/goniometer stages for accurate alignment of the system and for scanning azimuth and

elevation angles by the computer. In addition, high-resolution 3D datasets could be generated by mechanically scanning the FOV of the TCSPC system [35]. This feature was implemented in a LabView application allowing low speed scanning.

2.4 Detection setup

The collected photons were fed to the detection setup using a GRIN fibre to avoid mode dispersion, which would reduce the range resolution. The detection setup used a SPAD detector (PDM Series, Micro Photon Devices S.r.l., Bolzano, Italy) with 100 μm diameter, <250 dark counts/s, 87 ns detector dead-time and <50 ps timing jitter. The collected photons were collimated onto a band pass filter (λ_c=834 nm, $\Delta\lambda$=3 nm FWHM) and subsequently focussed on the SPAD detector via achromatic lenses. The band pass filter reduced the background count rate and only a small part of the radiation emitted from the SC fibre laser was utilised. The band pass filter was exchangeable allowing for spectral investigations. Aluminium housing enclosed the detection setup to eliminate stray light.

The NIM (Nuclear Instrumentation Module [36]) pulse from the SPAD module was used to trigger the timing acquisition hardware (PicoHarp300, PicoQuant GmbH, Berlin, Germany), measuring the time since the last electrical sync pulses from the SC fibre laser for each collected photon. Data were collected for 100 ms up to 100 s depending on the application and signal level, and typically 4 ps time resolution per bin was used for histograms. Discriminator detection thresholds on both channels were chosen to minimise the system (instrument) response function (IRF). Data acquisition software (PicoQuant GmbH) was utilised to collect histograms, which were subsequently analysed off-line on a PC using in-house developed software written in MATLAB.

3 Range profiling

In TCSPC range profiling, the TOF condition is used to determine the range based on the time between the detection of a single photon and the last laser pulse sync signal. Successively, a histogram representing the range profile can be constructed from photon arrival times, as shown in Figure 2. Only a small part of the emitted laser pulses (approx. <5%) is used in order to avoid detector 'pile-up' effects and fulfil the Poisson statistics requirements [7]. Consequently, a high PRF is required in order to build up histograms within reasonable integration times.

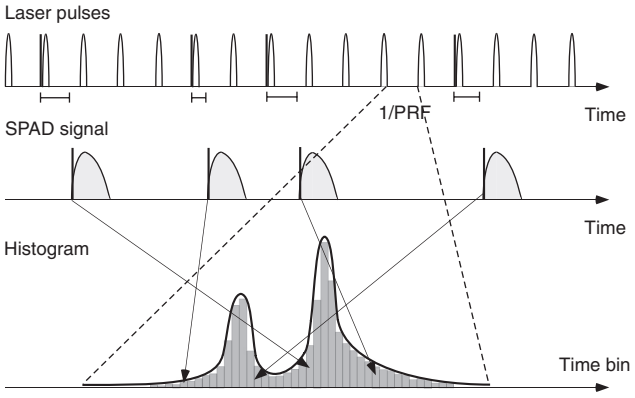

Figure 2 Principle of TCSPC range profiling showing the emitted laser pulses at MHz rates, detection of single photons using a SPAD detector and construction of a histogram based on measuring the time between the SPAD detections and the laser pulse sync signals.

In TCSPC range profiling, the ambiguity distance is given by the pulse-to-pulse interval of the laser which is, for example, 3.75 m in the case of 25 ns pulse intervals (40 MHz PRF). Methods for absolute ranging based on pseudo-random pulse trains have been presented [37]. The range resolution is characterised by the IRF, determined by the total system timing jitter. Using SPAD detectors and dedicated timing hardware subcentimetre resolution is obtainable, as shown in this study. The range resolution of the used TCSPC range profiling system has successively been improved compared with previously performed experiments [38–40]. In the following, we focus on the results obtained by the present setup providing subcentimetre range resolution. Only examples are provided in this work, and for more technical details we refer to previously published results.

3.1 System performance

The system performance was characterised in short range indoor experiments. The IRF of the system was determined using a convex Au mirror or a flat Lambertian surface. The experimental IRF could be fitted to the following analytical function (Figure 3) in analogy with Pellegrini et al. [5]:

$$y=\begin{cases}\exp\left(-\dfrac{(t-t_0)^2}{2w^2}\right), & t<t_1\\ \exp\left(-\dfrac{(t-t_1)^2}{2w^2}\right)\left[a\exp\left(-\dfrac{t-t_1}{\tau_1}\right)+b\exp\left(-\dfrac{t-t_1}{\tau_2}\right)\right], & t>t_1\end{cases} \quad (1)$$

with

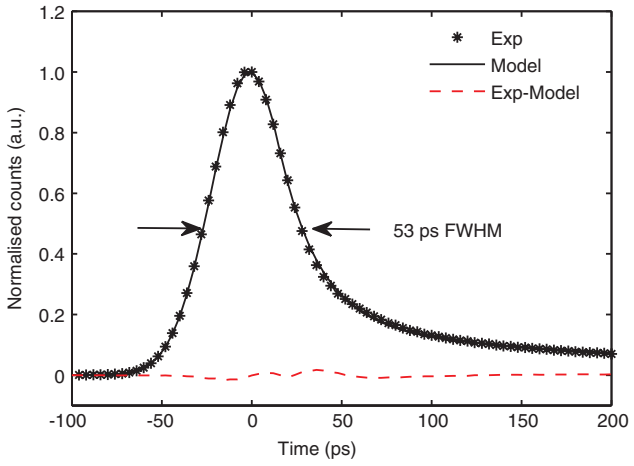

Figure 3 Instrument response function (IRF) for the TCSPC range profiling system determined by measuring the response from a convex Au metallic mirror at 53 m distance. The graph shows the experimental (stars), the model IRF (solid) and the subtracted signals (dash, experimental model).

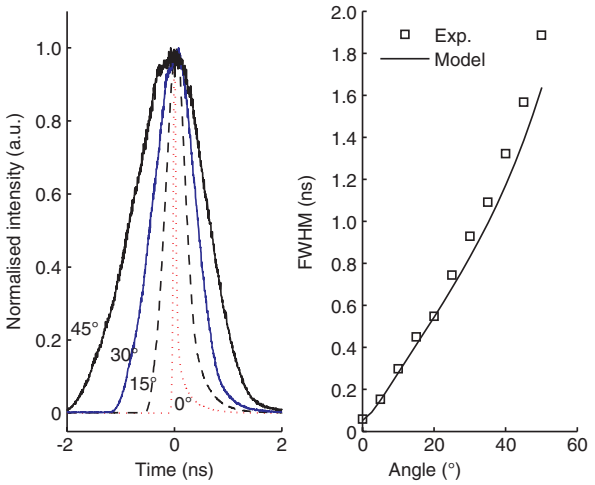

Figure 4 Pulse response from a flat Lambertian surface at varying angles of incidence (0° red dots, 15° black dash, 30° blue solid, 45° black solid, left). Experimental and theoretical pulse width (FWHM) as a function of angle of incidence (right).

$$a+b=1 \text{ and } \tau_2=\frac{b}{\left(\frac{t_1-t_0}{w^2}-\frac{a}{\tau_1}\right)} \tag{2}$$

including the five fitting parameters (t_0, t_1, w, a and t_1). Good agreement between the experimental and model IRF was obtained using a least square fit providing an error <1.5%. The FWHM of the IRF was measured to 53 ps, which corresponds to a range resolution of approximately 8.5 mm.

3.2 Geometrical targets

The studied geometrical shapes included a flat surface (which could be rotated), a variable step between two flat surfaces, cones with different dimensions and spheres having different reflectance ρ. The geometrical objects were placed at 34 m (flat screen) or 82 m distance (cones and spheres) from the TCSPC system and the wide FOV setup was used for the measurements. The flat surface was placed on a rotational stage to study the effect of altering the angle of incidence of the laser radiation with respect to the surface normal. To verify the range resolution of the system, a step between two surfaces was studied in addition to scanning the beam laterally over the step. The painted cones (ρ=0.3) had dimensions (base × height) of 9×40, 20×30 and 30×30 cm, and the diameter of the spheres was 14 cm. One sphere was painted white (ρ=0.3) and the other with metallic colour having a large specular component (ρ>0.9). All objects were carefully aligned towards the TCSPC system.

Figure 4 shows a typical pulse broadening when a plane surface is tilted. In this case, the beam radius is much smaller than the surface area when the angle of incidence θ=0°, that is, the laser beam is parallel with the surface normal. Varying the angle of incidence of the plane surface from 0° to 50° causes a pulse broadening from 0.05 ns (close to the IRF) to 1.9 ns. In addition to the experimental results, the theoretical pulse shape, based on the model IRF above convolved with the impulse response for a plane Lambertian surface, is depicted showing a calculated pulse broadening because of the alteration in geometry [41, 42]. Using this simple model, good agreement with the experimental results was obtained. The deviation at a larger angle of incidence may be attributed to slight inaccuracies in alignment and beam dimension on the surface.

The depth resolution was studied measuring the pulse response from the edge of two partially overlapping flat surfaces separated in distance ranging from 30 mm down to 5 mm. The 30 mm distance resulted in two well separated peaks. At 5 mm distance between the plane surfaces a double peak structure was still observable, indicating that there were two surfaces even though they were not fully resolved. This is in agreement with the narrow IRF predicting a resolution of 8 mm from the TOF relation. Similarly, mechanical scanning of the beam across the two surfaces separated by 5 mm in distance results in an evident step considering a two-dimensional (2D) data representation (scan position vs. depth), as is presented in Figure 5.

In addition to the investigated flat surface, pulse broadening from conical and spherical shaped

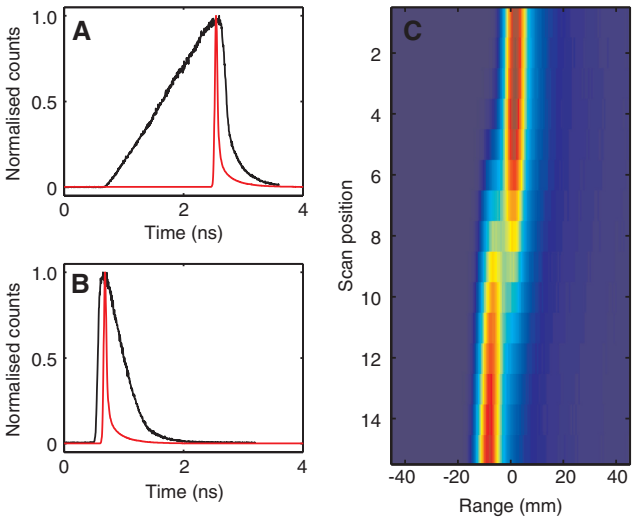

Figure 5 Pulse response from a cone, base × height, 20×30 cm (A), and sphere, radius 30 cm (B). The red line corresponds to the TCSPC system IRF function. Range profiles as a function of scan position across a step between two flat Lambertian plates separated by 5 mm in distance. The colour scale is proportional to count rate per bin.

geometries was also examined. Depending on the conical half angle, a broadening of the pulse shape can be observed, as shown in Figure 5A, for a cone (base × height, 20×30 cm). Here the linewidth increases to 282 ps in comparison to the 53 ps system IRF. The narrowing of the conical shape (9×40 cm) reduces the number of photons reflected towards the system causing a lower signal-to-noise ratio in the signal, as anticipated. With knowledge of the FOV and the target distance, the cone angle can be determined from the increase of the signal with distance [40]. Another example showing the influence of the surface geometry is the case of a Lambertian reflecting sphere with a 14 cm radius (Figure 5B). In this case, the linewidth was 296 ps (FWHM) and the peak shape is determined by the sphere radius relative to the FOV. For a sphere with a specular surface, primarily surfaces perpendicular to the laser beam would be reflecting back towards the system, limiting the possibility to draw conclusions about the shape. A narrow pulse shape (72 ps FWHM) is observed for a specular sphere with the same radius as the presented Lambertian diffusively reflecting surface sphere, which is in agreement with theoretical models [42].

As exemplified in the experimental results, the reflective properties, geometry and size relative to the illuminating beam of the studied objects have a large influence on the measured range profile. For a more detailed discussion on this issue, we refer to results presented in a previous study [40].

3.3 Long range reflector characterisation

Long range outdoor experiments were demonstrated by studying the range profile from an optical rifle scope and a road sign. In this case, the range was 750 m and measurements were performed with the monostatic narrow FOV transceiver in full daylight conditions. The background signal was reduced by spectral and spatial filtering (narrow FOV). In addition, turbulence studies using TCSPC range profiling have been carried out using a horizontal propagation path close to ground [43].

The rationale for these experiments was to investigate if high-resolution range profiling using acceptable integration times were achievable at a kilometre range. The objects studied here included reference objects (corner cube retro-reflector, plastic reflex), road signs and optical assemblies such as rifle scopes, focussing on the issue whether TCSPC range profiles can be used to classify an interrogated object using optical augmentation in a security application. Critical issues in long distance range profiling in daylight concern high background count rates, required integration times, distortion and broadening of the IRF because of high count rates and influence from turbulence effects.

The signal was registered from a corner cube retro-reflector (12.5 mm aperture) at 1.3 km distance using integration times varying between 100 ms and 10 s. A slight broadening of the histogram (61 ps FWHM) was observed compared with indoor measurements (53 ps FWHM). Several effects may contribute to this broadening. Both the position and the width of the IRF depend on the count rate, although with the thin junction SPAD detector used in this study this effect is less pronounced than with older thick junction SPAD detectors [44]. Thus, changes in average count rate and count rate fluctuations generated by turbulence-induced scintillations cause temporal broadening of the measured signal. Another source of temporal broadening is atmospheric scattering [45]. Typically, the contribution from the background was 20 to 100 kcps (kilo counts/s) without causing any limitation in retrieving histograms from different objects at a 750 m range. The signal-to-background ratio was of the order 28 to 30 dB. Pulse broadening because of slant surfaces was investigated by comparing the linewidth from two road signs, one directed with the surface perpendicular to the TCSPC system and one rotated 45°. Rotating the road sign caused an increase in the linewidth from 57 ps to 110 ps in agreement with the indoor results presented above for a flat surface.

In Figure 6, the observed TCSPC range profile from a road sign and a commercial rifle scope is shown, clearly

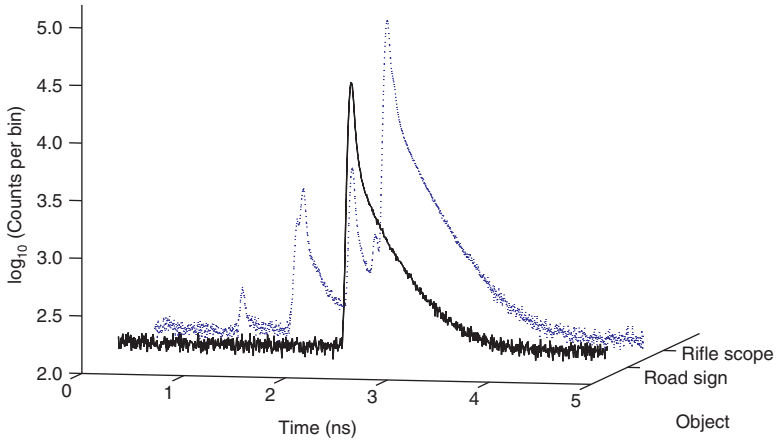

Figure 6 Time-correlated single-photon counting signals from a road sign (black) and a rifle scope (blue) at 750 m range in daylight conditions. The road sign was rotated 45° relative to normal incidence and the rifle scope was aimed at the TCSPC system.

indicating the different pulse shapes. The road sign exhibits a single peak close to the system IRF, whereas the rifle scope gives a range profile consisting of several peaks originating from the front optical group, a reticle in a focal plane and the lens group from the ocular. It should be stressed that the detailed optical schematics was not known in this example, limiting the information that can be extracted from the TCSPC data. However, if information about the optics is available modelling can be used to predict the TCSPC response [34].

Previously long range outdoor experiments were performed using a TCSPC laser radar system having a slightly lower range resolution focussing on the influence from turbulence effects on the single photon signal [38, 43]. Signal statistics, turbulence effects and influence from the background were analysed studying retro-reflecting objects at a 1080 m range, suggesting that integration times <100 ms were obtainable. Moreover, a novel method based on the co-variance of the signal which can be used in situations with low count rates and high temporal resolution for determining the scintillation index using TCSPC data was proposed [46]. In addition, this scheme was compared with a traditional approach based on fitting theoretical probability density functions to the intensity fluctuations capable of including detector dead-time effects and to be used at higher count rates.

4 Reflective tomography

4.1 Theory

In reflectance, TCSPC tomography 2D images are reconstructed from range profiles registered for different view angles of a studied opaque object. The principle is depicted in Figure 7. Based on the scheme for filtered back-projection (FBP) using the inverse Radon transform, the tomographic image can be reconstructed. Mathematically, the 2D object can be expressed as [47]:

$$g(x,y)=\sum_{i=1}^{m} q(z\cos\theta_i + x\sin\theta_i)\Delta\theta \tag{3}$$

where

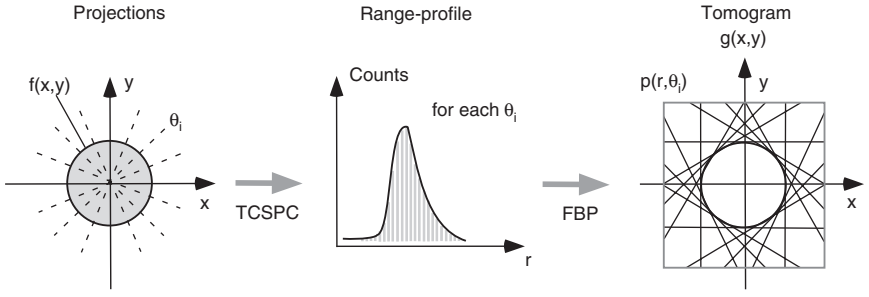

Figure 7 Schematic showing the principle of reflectance TCSPC tomography with projections and range profiles for each angle of incidence θ_i, and the corresponding tomogram after the filtered back projection (FBP) transform.

$$q(r,\theta)=\mathcal{F}^{-1}(f\mathcal{F}\{p(r,\theta_i)\}) \quad (4)$$

and $\mathcal{F}$, $\mathcal{F}^{-1}$ denotes the forward and inverse Fourier transform, respectively, r is the distance along the measurement direction with zero at the rotation centre of the studied object (not a polar coordinate), $p(r,\theta_i)$ is the range profile for each rotation angle θ_i and f is a filter function. Here it was assumed that the rotation axis is parallel to the y-axis.

The filter function, f, was chosen to be a generalised ramp function according to:

$$f(\omega)=|\omega|\cdot e^{-\xi|\omega|^a} \qquad 0\le|\omega|\le\pi \quad (5)$$

and $\xi=\left|\frac{1}{\omega_c}\right|^a$ with ω_c defining the cut-off frequency and a an adjustable parameter. Typical values used in this work to reduce the high frequency components were $a = 3.4$ and $\omega_c = \pi/4$. The values need to be optimised based on the IRF of the measurement system. Further improvement of the tomographic images was obtained by removing artefacts from strongly reflecting features of the studied opaque object that cause linear features stretching through the reconstructed image. The influence from these artefacts can be partly removed by using the 'convex hull' method where the first response (opaque surface) at each angle from the object is used to create an image mask outside which the response is known to be zero. Subsequently the tomographic image can be multiplied with the created mask to remove linear features stretching past the borders of the object. It should be stressed that in the scheme described above only opaque objects have been considered, although the tomographic method is applicable to partial reflecting surfaces within the TCSPC range profile. Critical issues regarding the quality of the reconstructed tomogram include defining the centre of rotation, applied angular resolution and the used angular projection sector.

4.2 Experimental measurements

In the TCSPC tomography experiments, objects were placed at 53 m distances on a rotational stage allowing azimuth angles from -170° to +170° using a typical step size of 1°–5°. A step and stare mode was used to register range profiles (histograms) for each angle step controlled by a LabView application. Histograms were stored on a computer for off-line data processing and tomographic image reconstruction. TCSPC tomography was exemplified by studying an object possessing several flat surfaces, a metallic optical rail (girder) and a model boat.

In Figure 8, the result from TCSPC tomography of a metal girder placed on the rotational stage is shown. The TCSPC range profiles are arranged in a 2D matrix with a column corresponding to a specific angular projection θ_i. In this case, the angular resolution was 1° and the angular sector ±170°. An example of an individual range profile corresponding to θ_i = 10° projection angle is depicted. After performing the inverse Radon transform of the range/projection matrix, the reflectance tomogram is obtained (Figure 8B).

A more complicated studied object is a boat model (44 × 23 × 35 cm, length × width × height) viewed from the side. The strongest range profile signals from the boat model were obtained in projections with the long side of the model directed towards the TCSPC system with strong contributions from the hull, the cabin wall and sails. The corresponding tomogram obtained after FBP is depicted in Figure 9A. As observed, there are still some artefacts present in the tomogram because of strong specular signals in the range/projection matrix and 3D reflecting features. Moreover, limitations in the angular resolution and the covered angular sector may also generate artefacts.

In Figure 9B, the tomographic image of the model boat is enhanced by applying the 'convex hull' method. Here the first return in the range profiles is used to create a mask, which is subsequently multiplied with the tomogram. Other examples such as limited angular section and

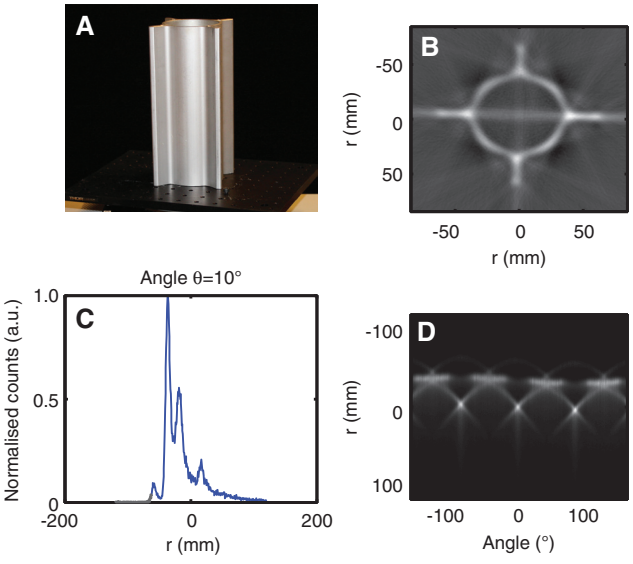

Figure 8 Time-correlated single-photon counting tomography of a metal girder (A, B). An example showing the angular range profile (C) and all angular projections (D) are depicted in the lower figures. The grey scale is proportional to the normalised number of photon counts.

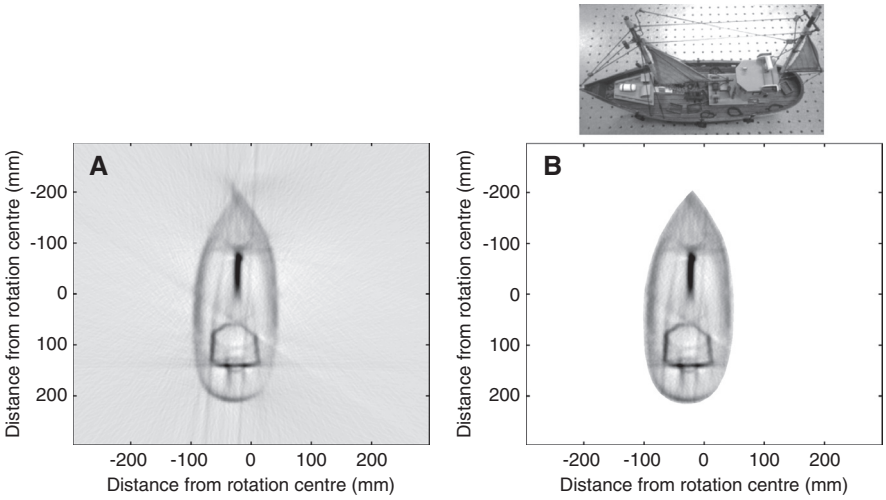

Figure 9 Reconstructed tomographic TCSPC image of a model boat (A) and after applying a mask based on the convex hull, that is, the first return surface in the range profiles (B). Photograph showing the model boat (upper right).

background contribution have to be taken into account to reconstruct the tomographic image, and have previously been presented [47]. In particular, the case with a TCSPC sensor on a moving airborne platform studying an object on the ground was considered and found to be difficult.

5 Discussion and conclusions

The time-correlated laser radar exhibits excellent properties for high-resolution range profiling and 3D imaging at short and long distances. Mechanical scanning in the lateral plane or the use of SPAD detector arrays provides 3D information about remote objects in a scene. One-dimensional range profiling provides a simple method to extract information about both non-cooperative and cooperative remote objects. The present study has shown a TCSPC system with subcentimetre range resolution providing opportunities to extract information about remote objects in order to facilitate classification. Using TCSPC, pulse shape feature information about the geometric objects can be obtained [40]. The extreme range resolution of TCSPC LADAR makes it possible to perform experiments using laboratory scale models relevant for scaling to data expected with linear-mode laser radar systems for the identification of large-scale objects, allowing testing of possible system performance in a simple and inexpensive way [48].

Non-cooperative objects pose a particular difficult task, because neither the orientation nor the number of reflecting surface are *a priori* known, requiring sophisticated signal processing methods to be applied [14, 15]. This is particularly evident in situations interrogating objects giving rise to a low number of detectable photon counts. It should also be emphasised that perturbations from atmospheric turbulence and high background contributions further complicate the problem. Considering cooperative objects, by contrast, information about the studied objects can be utilised in the analysis of TCSPC waveforms.

Moreover, reflectance TCSPC tomography can be used to create 2D images from rotating opaque objects, as presented in this work. If the axis of rotation is known and the angular resolution and projection sector is adequate, tomographic reconstructions can be generated. So far, the method has been tested at short indoor distance and further experiments at a longer range and in daylight are required to evaluate the method. In analogy to the rotating target, the opposite situation can be imagined where the TCSPC sensor is moving about an object of interest. In this case, the background, the covered angular sector and the changing distance to the rotation axis are issues that need to be considered [47]. The present laboratory results indicate that these complications can be difficult to overcome, and improved methods are required to apply reflective tomographic laser radar for this particular application.

In addition to laterally unresolved range profiling and reflectance tomographic imaging, TCSPC laser radar can generate high resolution 3D data using a step-and-stare mode, although this scheme has the disadvantage of long scanning times with the present TCSPC setup [35]. However, point-to-point high-resolution range-resolved studies are of importance in several applications. Concerning non-cooperative objects, classification of objects

detected by optical augmentation was provided as a possible application. If the target type is known, by contrast, information about the pulse shape can be utilised to also extract information at longer distance. The inherent feature of photon counting and low laser power emission makes TCSPC covert, in particular considering the possibility to use sparse waveforms and pseudo-random pulse streams. One example in this respect is absolute range finding [16, 45]. Other critical issues related to the performance of the method include whether the studied objects can be considered to be stationary in relation to the integration time.

The present results were achieved using an 800–900 nm wavelength region, whereas a system operating around 1550 nm is preferable from eye safety issue considerations [49]. SNSPD devices, although complicated, show very interesting features for future TOF range profiling and imaging systems. Moreover, future developments of GM and SPAD single-photon array detectors are anticipated enabling the development of flood illumination systems operating in the SWIR wavelength region [21–23, 50]. Among the novel imaging techniques, the CS method may provide an interesting alternative for future 3D imaging application based on single-pixel detectors [27].

In conclusion, TCSPC range profiling and reflectance tomography exhibits interesting features for short and long range applications. Range profiling with subcentimetre resolution is achievable at longer distances in full daylight. Tomographic information can be extracted from remote rotating objects and used to extract object features.

Acknowledgements: This work was supported by the Swedish Armed Forces and the Security Link Strategic Research Centre at Linköping University. Mr. Tomas Olofsson and Mr. Carl Brännlund are gratefully acknowledged for carrying out parts of the optical reflectance TCSPC tomography experiments.

Received January 10, 2014; accepted February 13, 2014; previously published online March 10, 2014

References

[1] P. F. McManamon, Opt. Eng. 51, 060901-13 (2012).
[2] M. A. Itzler, R. Ben-Michael, C. F. Hsu, K. Slomkowski, A. Tosi, et al., J. Mod. Opt. 54, 283–304 (2007).
[3] F. Villa, B. Markovic, S. Bellisai, D. Bronzi, A. Tosi, et al., IEEE Photon. J. 4, 795–804 (2012).
[4] G. S. Buller and A. M. Wallace, IEEE J. Sel. Top. Quant. Electr. 13, 1006–1015 (2007).
[5] S. Pellegrini, G. S. Buller, J. M. Smith, A. M. Wallace and S. Cova, Meas. Sci. Technol. 11, 712–716 (2000).
[6] M. A. Albota, R. M. Heinrichs, D. G. Kocher, D. G. Fouche, B. E. Player, et al., Appl. Opt. 41, 7671–7678 (2002).
[7] G. Buller and R. Collins, Meas. Sci. Technol. 21, 012002-28 (2010).
[8] M. A. Itzler, X. Jiang, M. Entwistle, K. Slomkowski, A. Tosi, et al., J. Mod. Opt. 58, 174–200 (2011).
[9] C. Niclass, M. Gersbach, R. Henderson, L. Grant and E. Charbon, IEEE J. Sel. Top. Quant. Electr. 13, 863–869 (2007).
[10] A. Tosi, A. Della Frera, A. Bahgat Shehata and C. Scarcella, Rev. Sci. Instr. 83, 013104-8 (2012).
[11] R. A. Lamb, Proc. SPIE 7483, 748308-15 (2009).
[12] G. S. Buller, R. D. Harkins, A. McCarthy, P. A. Hiskett, G. R. MacKinnon, et al., Rev. Sci. Instr. 76, 083112-7 (2005).
[13] A. Wallace, G. Buller, R. Sung, R. Harkins, A. McCarthy, et al., J. Opt. A Pure Appl. Opt. 7, S438–S444 (2005).
[14] A. M. Wallace, J. Ye, N. J. Krichel, A. McCarthy, R. J. Collins, et al, EURASIP J. Adv. Sign. Process. 2010, 896708-12 (2010).
[15] J. Ye, A. M. Wallace, A. Al Zain, J. Thompson and J. Parall, Distr. Comput. 73, 383–399 (2013).
[16] N. J. Krichel, A. McCarthy and G. S. Buller, Opt. Express 18, 9192–9206 (2010).
[17] N. J. Krichel, A. McCarthy, I. Rech, M. Ghioni, A. Gulinatti, et al., J. Mod. Opt. 58, 244–256 (2011).
[18] M. Richard and W. Davis, Linc. Lab. J. 15, 37–60 (2005).
[19] J. Degnan, R. Machan, E. Leventhal, D. Lawrence, G. Jodor, et al., Proc. SPIE 6950, 695007-9 (2008).
[20] T. K. Cossio, K. C. Slatton, W. E. Carter, K. Y. Shrestha and D. Harding, IEEE J. Sel. Top. Appl. Earth Observ. Rem. Sens. 3, 672–688 (2010).
[21] P. Yuan, R. Sudharsanan, X. Bai, P. McDonald, E. Labios, et al., Proc. SPIE 8379, 837902-12 (2012).
[22] M. A. Itzler, M. Entwistle, M. Owens, K. Patel, X. Jiang, et al., Proc. SPIE 8033, 80330G-12 (2011).
[23] P. Yuan, R. Sudharsanan, X. Bai, E. Labios, B. Morris, et al., Proc. SPIE 8731, 87310X-10 (2013).
[24] A. Tosi and F. Zappa, Proc. SPIE 8899, 88990D-9 (2013).
[25] P. A. Hiskett and R. A. Lamb, Proc. SPIE 8033, 80330F-17 (2011).
[26] G. A. Howland, P. B. Dixon and J. C. Howell, Appl. Opt. 50, 5917–5920 (2011).
[27] G. A. Howland, D. J. Lum, M. R. Ware and J. C. Howell, Opt. Express 21, 23822–23837 (2013).
[28] A. McCarthy, N. J. Krichel, N. R. Gemmell, X. Ren, M. G. Tanner, et al., Opt. Express 21, 8904–8915 (2013).
[29] S. Chen, D. Liu, W. Zhang, L. You, Y. He, et al., Appl. Opt. 52, 3241–3245 (2013).
[30] M. Ren, X. Gu, Y. Liang, W. Kong, E. Wu, et al., Opt. Express 19, 13497–13502 (2011).
[31] G. S. Buller, R. J. Collins, P. J. Clarke, N. J. Krichel, A. McCarthy, et al., Proc. SPIE 7945, 79452M-9 (2011).
[32] P. A. Hiskett, R. A. Struthers, R. Tatton and R. Lamb, Proc. SPIE 8542, 854214 (2012).
[33] T. Merhav, V. Savuskan and Y. Nemirovsky, Proc. SPIE 8896, 88960H-13 (2013).

[34] L. Sjöqvist, L. Allard, M. Henriksson, P. Jonsson and M. Pettersson, Proc. SPIE 8898, 88980K-14 (2013).
[35] O. Steinvall, L. Sjöqvist and M. Henriksson, Proc. SPIE 8375, 83750C-14 (2012).
[36] US Nuclear Instrumentation Module Committee, US Department of Energy, DOE/ER-0457T (1990).
[37] P. Hiskett, C. S. Parry, A. McCarthy and G. S. Buller, Opt. Express 16, 13685–13698 (2008).
[38] L. Sjöqvist, C. Grönwall, M. Henriksson, P. Jonsson and O. Steinvall, Proc. SPIE 7115, 71150G-12 (2008).
[39] L. Sjöqvist, M. Henriksson, P. Jonsson and O. Steinvall, Proc. SPIE 6738, 67380N-12 (2007).
[40] O. Steinvall, L. Sjöqvist, M. Henriksson and P. Jonsson, Proc. SPIE 6950, 695002-13 (2008).
[41] C. Grönwall, O. Steinvall, F. Gustafsson and T. Chevalier, Opt. Eng. 46, 106201-11 (2007).
[42] O. Steinvall, Appl. Opt. 39, 4381–4391 (2000).
[43] M. Henriksson and L. Sjöqvist, Proc. SPIE 8187, 81870N-12 (2011).
[44] R. E. Warburton, A. McCarthy, A. M. Wallace, S. Hernandez-Marin, S. Cova, et al., Opt. Express 15, 423–429 (2007).
[45] R. A. Lamb and P. Hiskett, in IEEE '2011 Saudi International Electronics, Communications and Photonics Conference (SIECPC)' (KACST, Saudi Arabia, 2011) pp.1–6.
[46] M. Henriksson and L. Sjöqvist, Opt. Eng, 58, in press, (2014).
[47] M. Henriksson, T. Olofsson, C. Grönwall, C. Brännlund and L. Sjöqvist, Proc. SPIE 8542, 85420E-9 (2012).
[48] O. Steinvall, M. Elmqvist, T. Chevalier and C. Brännlund, Proc. SPIE 8542, 85420I-17 (2012).
[49] A. McCarthy, X. Ren, A. Della Frera, N. R. Gemmell, N. J. Krichel, et al., Opt. Express 21, 22098–22113 (2013).
[50] C. Niclass, M. Soga, H. Matsubara, S. Kato and M. Kagami, IEEE J. Solid State Circ. 48, 1–2 (2013).

Lars Sjöqvist is a Research Director in Laser Technologies. He received his MSc in Electro-engineering and Applied Physics in 1987, and his PhD in Chemical Physics in 1991, from Linköping University. Previous work includes magnetic resonance spectroscopy and imaging in different medical applications. Presently, he is working as a Research Director at the Swedish Defence Research Agency, Division of Sensor and EW Systems, Laser Systems Group, where he is studying laser technologies, single-photon counting techniques, new photonics components for active optics, laser countermeasures including system analysis, and laser propagation effects. He is author or co-author of approximately 70 journal articles and conference papers and more than 65 internal reports. He also holds a position as Associate Professor in the Department of Physics at Linköping University. He is a member of SPIE, the Optical Society of America, and the European Optical Society.

Markus Henriksson graduated from Chalmers University of Technology, Gothenburg, Sweden, in 2002 with a Master's Degree in Engineering Physics. He then joined the Laser Systems Group at FOI, the Swedish Defence Research Agency. In 2010, he received his PhD in Physics from the Royal Institute of Technology (KTH), Stockholm, Sweden. His research interests include optical parametric oscillators, laser radar, laser beam propagation and laser-based countermeasures.

Per Jonsson received his PhD in Photonics from the Royal Institute of Technology (KTH), Stockholm, Sweden in 2002. The title of his thesis is 'Generation, detection and application of single photons'. Dr. Jonsson joined FOI, the Swedish Defence Research Agency in 2002 and is presently a Senior Scientist. His main research area at FOI is detection of biological and chemical warfare agents with laser systems. Dr. Jonsson has also worked in other fields of research at FOI including coherent laser radar, free optical communication, including the so-called quantum cryptography and single-photon detection in electronic warfare applications.

Ove Steinvall received his MS Degree in Physics at the University of Uppsala in 1969. He was then employed by the National Defence Research Establishment (FOA, now FOI) in 1969. He received his PhD in 1974 in Lasers and Electro-optics from the Chalmers Institute of Technology. Since 1977, he has been leading the Laser Group, from 1994 he has been a Department Head and from 2007 to 2009 he was Head of the Optronic Systems Department. He now holds the position as a Research Director in Laser Systems. His research activities include lasers, lasers for countermeasures, laser warning, laser radar/lidar including systems for imaging and mapping, free space laser communications and ocean/atmospheric optics. He is author or co-author of approximately 100 conference and journal articles and approximately 300 internal reports. Dr. Steinvall is a fellow of SPIE, the Society for Photo-optical Instrumentation Engineers, and a member of the Optical Society of America, the Swedish Optical Society and the Royal Academy of Military Sciences. He has received three national rewards for his laser work. He has also received the NATO Scientific Achievement Award (SET-077). He has been the Conference Chair for several laser conferences. He is an expert in EDA Captech IAP3 and holds a position as Associate Professor at the Chalmers Institute of Technology.